Electronic Supplementary Information

Efficient C_2H_2-selective separation in a microporous Zn(II)-based metal-organic framework via the dual-ligand strategy

Fan Yang,[a] Juan-Juan Xue,[a] Guang-Ping Lei,[b] Wen-Yan Zhang,[a] Guo-Ping Yang,*[a] and Yao-Yu Wang*[a]

[a] *Key Laboratory of Synthetic and Natural Functional Molecule of the Ministry of Education, Shaanxi Key Laboratory of Physico-Inorganic Chemistry, Xi'an Key Laboratory of Functional Supramolecular Structure and Materials, College of Chemistry and Materials Science, Northwest University, Xi'an 710127, P. R. China*

[b] *Research Center of Shanxi Province for Solar Energy Engineering and Technology, School of Energy and Power Engineering, North University of China, Taiyuan 030051, P. R. China.*

*Email: ygp@nwu.edu.cn; wyaoyu@nwu.edu.cn.

Content

S1. Materials and General Methods

All reagents and materials were obtained commercially and used as received without further purification. Elemental analyses of carbon, hydrogen and nitrogen were performed on a PerkinElmer 2400C elemental analyzer. Powder X-ray diffraction (PXRD) data were collected on a Bruker D8 ADVANCE X-ray powder diffractometer (Cu Kα, λ = 1.5418 Å) with 2θ (5−50°). Thermogravimetric analyses (TGA) were measured under a nitrogen stream employing the NETZSCH STA 449C microanalyzer thermal analyzer at a heating rate of 5 °C min^{-1}. The gas sorption isotherms were measured on Micrometrics ASAP 2020M sorption equipment. Breakthrough experiments were performed on a Quantachrome dynaSorb BT equipment.

S2. Experiment Section and Characterization

S2-1. Synthesis of 1

A mixture of $Zn(NO_3)_2$ $6H_2O$ (29.9 mg, 0.1 mmol), H_4L1 (22.5 mg, 0.05 mmol), Adenine(6.7 mg, 0.05 mmol) N,N-dimethylformamide (DMF, 4.0 mL), H_2O (2.0 mL), and CH_3CH_2OH (1.0 mL) was placed in a 15 mL bomb and heated at 105 ˚C for 72 h. The yellow block crystals (Fig. S1 and S2) were collected after cooling it to room temperature at a rate of 10 ˚C h^{-1}(48% yield based on H_4L1). After three days of the solvent exchange with acetone, adsorbent **1a** was obtained by activating at 373 K under vacuum for 6 h to remove the guest solvents. Anal. Calcd. (found) (%) for $[(Me)_2NH_2][Zn_{2.5}(L1)(Ade)(HCOO)]\cdot(DMF)_2(H_2O)_3$: C, 41.78 (41.53); H, 3.49 (3.65); N, 11.47 (11.62).

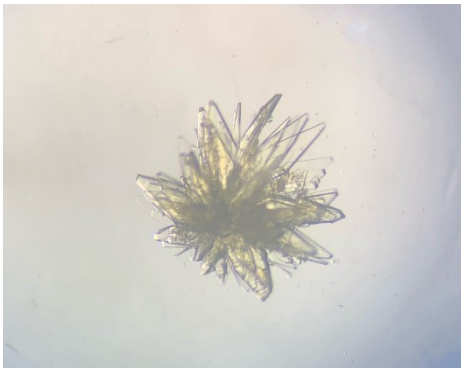

Fig. S1 Microscopy photograph of crystal morphology for MOF **1**.

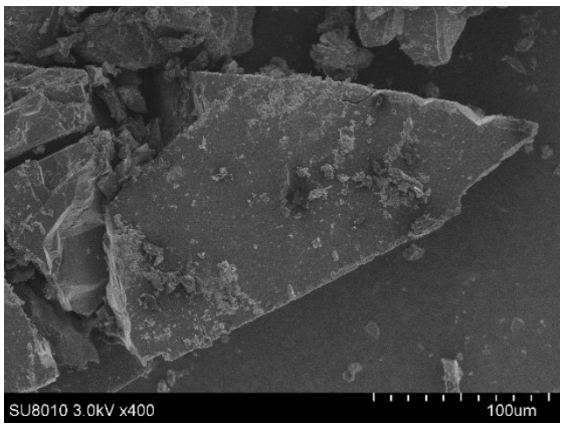

Fig. S2 SEM image of MOF **1**.

S2-2. Crystallographic Data Collection and Refinement

The single crystal structure of **1** was measured by single crystal X-ray diffraction (SCXRD) on Bruker SMART APEX II CCD diffractometer equipped with graphite monochromated Mo Kα radiation (λ = 0.710 73 Å) via ϕ/ω scan method. The diffraction data were corrected for Lorentz and polarization effects for empirical absorption based on multiscan. The structures were solved by the direct methods and refined by full-matrix least-squares refinements based on F^2. Anisotropic thermal parameters were applied to all non-hydrogen atoms. All hydrogen atoms of ligands were calculated and added at ideal positions. The disordered lattice molecules were refined by the SQUEEZE program. and this result is consistent to the results of TGA. Crystallographic calculations were performed using *Olex* 2 with 'XL' plug-ins.

Table S1. The crystallographic data of **1**.

Compound	**1**
Empirical formula	$C_{28}Zn_{2.5}N_6O_{12}H_{14}$
Formula mass	776.27
Crystal system	Triclinic
Space group	$P\bar{1}$
a [Å]	13.316(3)
b [Å]	13.775(3)
c [Å]	14.849(3)
α [°]	107.422(4)
β [°]	101.816(4)
γ [°]	95.038(4)
V [Å^3]	2511.1(9)
Z	2

ρ [g·cm^{-3}]	1.027
μ [mm^{-1}]	1.233
F [000]	763
θ [º]	1.733 - 25.976
Reflections collected / unique	13347 / 9553
Goodness-of-fit on F^2	0.975
Final R indices [$I>2\sigma(I)$]	R_1[a] = 0.0587, wR_2[b] = 0.1540
R indices (all data)	R_1[a] = 0.0931, wR_2[b] = 0.1710

[a]$R_1 = \sum||F_o|-|F_c||/\sum|F_o|$; [b]$wR_2 = [\sum w(F_o^2-F_c^2)^2/\sum w(F_o^2)^2]^{1/2}$

Table S2. Selected bond lengths [Å] and angles [°] for **1**.

Compound 1			
Zn(1)-Zn(1)#1	3.0456(13)	O(9)#1-Zn(1)-O(2)	157.06(16)
Zn(1)-O(3)	2.040(4)	O(8)-Zn(2)-N(10)#2	99.85(15)
Zn(1)-O(4)#1	2.058(3)	O(13)#3-Zn(2)-O(8)	101.57(16)
Zn(1)-O(2)	2.058(4)	O(13)#3-Zn(2)-N(10)#2	108.93(18)
Zn(1)-N(12)	1.996(4)	O(5)-Zn(2)-O(8)	117.4(2)
Zn(1)-O(9)#1	2.040(4)	O(5)-Zn(2)-N(10)#2	129.0(2)
Zn(2)-O(8)	1.982(4)	O(5)-Zn(2)-O(13)#3	96.85(18)
Zn(2)-N(10)#2	1.988(4)	O(8)#4-Zn(3)-O(8)#3	180.00(12)
Zn(2)-O(13)#3	1.968(4)	O(8)#3-Zn(3)-N(20)#7	90.17(14)
Zn(2)-O(5)	1.934(4)	O(8)#3-Zn(3)-N(20)#6	89.83(14)
Zn(3)-O(8)#4	2.148(3)	O(8)#4-Zn(3)-N(20)#7	89.83(14)
Zn(3)-O(8)#3	2.148(3)	O(8)#4-Zn(3)-N(20)#6	90.17(14)
Zn(3)-O(1)	2.079(4)	O(1)-Zn(3)-O(8)#3	91.15(14)
Zn(3)-O(1)#5	2.079(4)	O(1)#5-Zn(3)-O(8)#3	88.85(14)
Zn(3)-N(20)#6	2.176(4)	O(1)#5-Zn(3)-O(8)#4	91.15(14)
Zn(3)-N(20)#7	2.176(4)	O(1)-Zn(3)-O(8)#4	88.85(14)
O(8)-Zn(3)#8	2.148(3)	O(1)-Zn(3)-O(1)#5	180.0
O(8)-C(89)	1.267(8)	O(1)#5-Zn(3)-N(20)#7	93.14(16)
O(4)-Zn(1)#1	2.058(3)	O(1)-Zn(3)-N(20)#7	86.86(16)
N(10)-Zn(2)#9	1.987(4)	O(1)#5-Zn(3)-N(20)#6	86.86(16)
O(13)-Zn(2)#3	1.968(4)	O(1)-Zn(3)-N(20)#6	93.14(16)
O(13)-C(36)	1.272(6)	N(20)#6-Zn(3)-N(20)#7	180.00(18)
O(5)-C(31)	1.186(9)	C(82)-O(3)-Zn(1)	135.1(4)
O(9)-Zn(1)#1	2.040(4)	Zn(2)-O(8)-Zn(3)#8	110.89(17)
O(9)-C(24)	1.275(7)	C(89)-O(8)-Zn(2)	115.8(4)
N(20)-Zn(3)#10	2.176(4)	C(89)-O(8)-Zn(3)#8	126.6(4)
O(3)-Zn(1)-Zn(1)#1	73.55(11)	C(36)-O(1)-Zn(3)	140.1(4)
O(3)-Zn(1)-O(4)#1	156.42(15)	C(82)-O(4)-Zn(1)#1	121.9(4)
O(3)-Zn(1)-O(2)	87.85(16)	C(25)-N(10)-Zn(2)#9	128.5(3)

O(3)-Zn(1)-O(9)#1	88.17(15)	C(28)-N(10)-Zn(2)#9	126.7(3)
O(4)#1-Zn(1)-Zn(1)#1	83.11(11)	C(28)-N(10)-C(25)	104.1(4)
O(4)#1-Zn(1)-O(2)	87.17(16)	C(24)-O(2)-Zn(1)	139.7(4)
O(2)-Zn(1)-Zn(1)#1	69.80(12)	C(28)-N(12)-Zn(1)	117.4(3)
N(12)-Zn(1)-Zn(1)#1	166.03(13)	C(28)-N(12)-C(29)	103.5(4)
N(12)-Zn(1)-O(3)	102.57(16)	C(29)-N(12)-Zn(1)	139.0(3)
N(12)-Zn(1)-O(4)#1	100.91(16)	C(36)-O(13)-Zn(2)#3	123.6(3)
N(12)-Zn(1)-O(2)	96.88(17)	C(31)-O(5)-Zn(2)	117.2(5)
N(12)-Zn(1)-O(9)#1	106.03(18)	C(24)-O(9)-Zn(1)#1	116.3(4)
O(9)#1-Zn(1)-Zn(1)#1	87.41(12)	C(25)-N(20)-Zn(3)#10	128.9(3)
O(9)#1-Zn(1)-O(4)#1	87.50(16)	C(30)-N(20)-Zn(3)#10	118.7(3)

Symmetry codes:#1 -x+1,-y+1,-z+1; #2 x,y-1,z; #3 -x+1,-y,-z; #4 x+1,y+1,z; #5 -x+2,-y+1,-z; #6 -x+1,-y+1,-z; #7 x+1,y,z; #8 x-1,y-1,z; #9 x,y+1,z; #10 x-1,y,z.

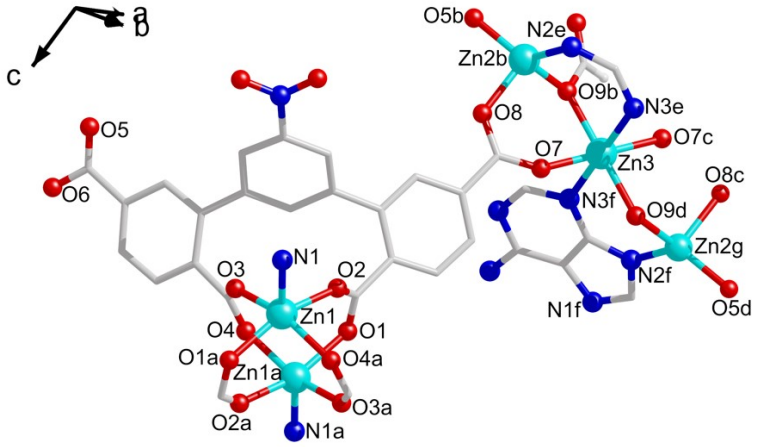

Fig. S3 Coordination environment of Zn^{2+} ions in **1**. Symmetric code: a 1-x, 1-y, 1-z; b 1-x, -y, -z; c 2-x, 1-y, -z; d 1+x, 1+y, z; e 1-x, 1-y, -z; f 1+x, y, z.

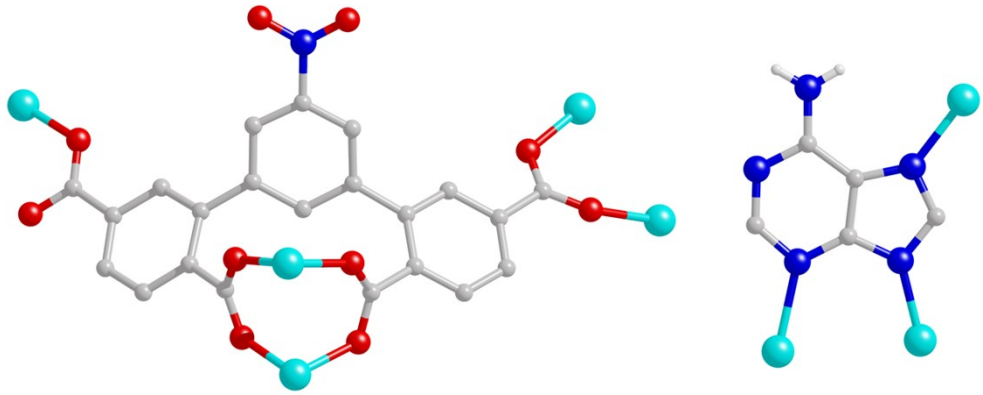

Fig. S4 Coordination mode of L1and ancillary ligand Ade in **1**.

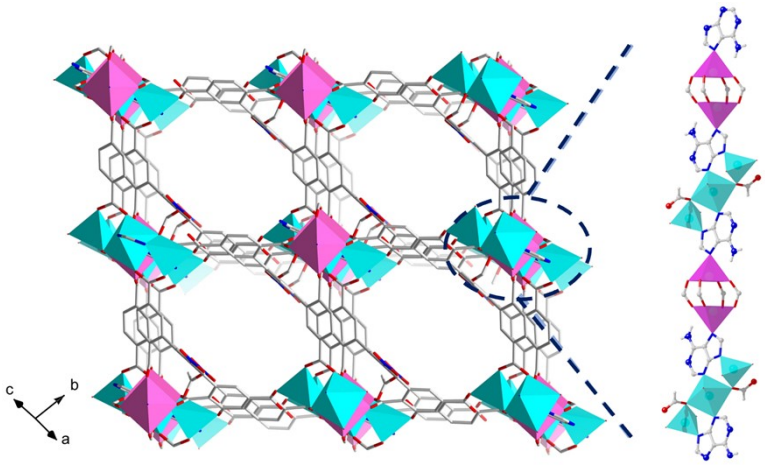

Fig. S5 3D porous network viewed along the [101] direction and the Zn-Ade linear chain.

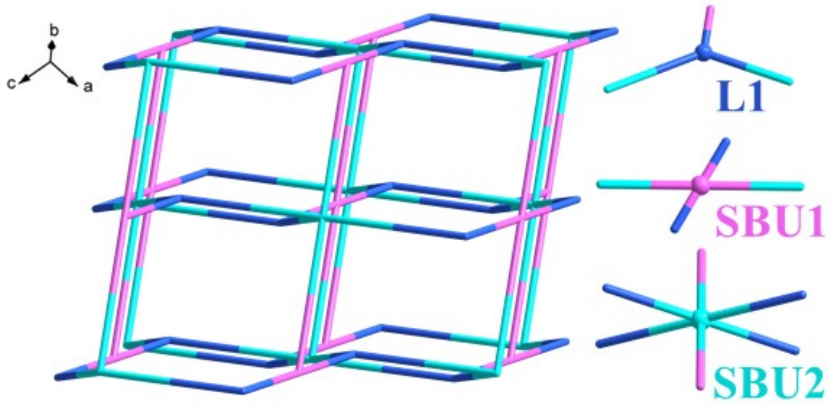

Fig. S6 Topological net viewed along the [121] direction.

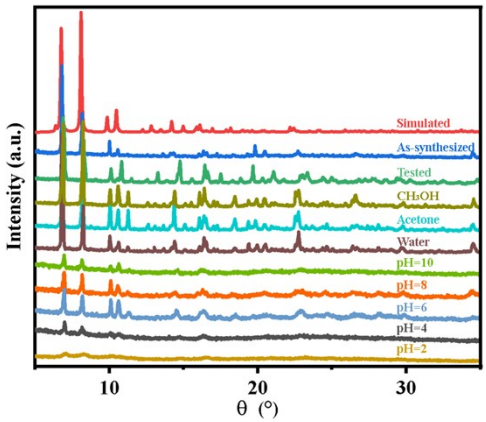

Fig. S7 PXRD patterns of simulated **1**, as-synthesized **1**, tested **1a** after adsorption, and **1** in different solvents for 12 h.

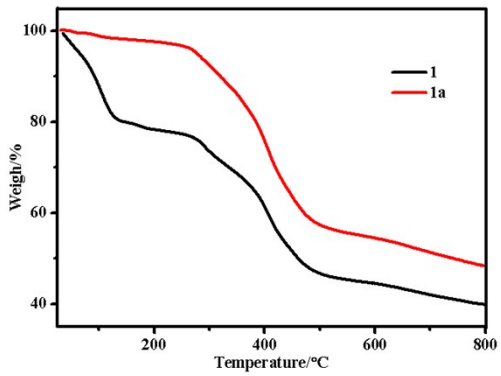

Fig. S8 TGA curve of as-synthesized **1** and adsorbent **1a**.

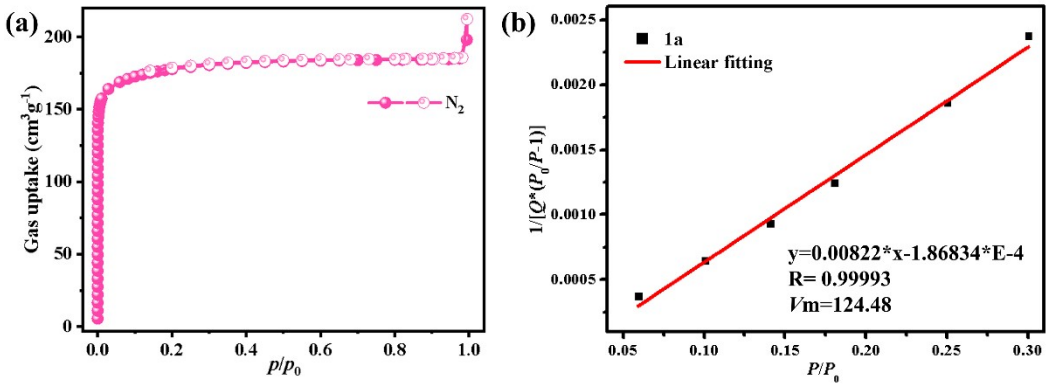

Fig. S9 (a) N_2 adsorption isotherms at 77 K of **1a**. (b) The BET surface area plot for **1a.**

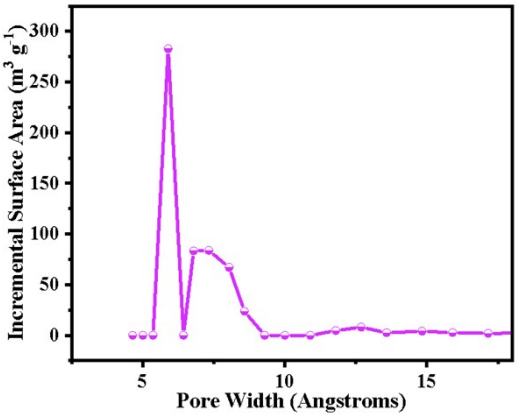

Fig. S10 The pore size distribution of **1a** (mainly at 5.8 and 7.3 Å), as calculated by Original Density Functional Theory.

S3. Gas Adsorption

Table S3. Comparison of C_2H_2 uptake amount and storage density of some MOF adsorbents for C_2H_2/CO_2 separation at 1 bar.

Adsorbent	Uptake amount ($cm^3\ g^{-1}$)	Storage density ($g\ cm^{-3}$)	Reference
ZJU-50a	192	0.24	S2
MIL-160	191	0.25	S3
Ni3-bdc-tpt	162.1	0.2	S4
UPC-200(Al)-F-BIM	144.5	0.11	S5
SNNU-45	134.0	0.13	S6
UTSA-74a	104	0.16	S7
1a	**100.8**	**0.12**	**This work**
SIFSIX-21-Ni	90.7	0.14	S8
CAU-10-H	89.8	-	S9
ZJU-74a	85.7	0.13	S10
ZNU-1	76.3	0.1	S11
SNNU-313-Cl	76.2	0.13	S12
JCM-1	75.0	0.12	S13
ZU-610	72.8	0.13	S14
UTSA-300a	69.5	0.13	S15
JNU-1	60.0	0.10	S16
ZrT-1-tetrazol	57.7	-	S17
$Ni_3(pzdc)_2(7Hade)_2$	52.9	0.12	S18
Cu^I@UiO-66-$(COOH)_2$	47.9	0.11	S19
CPL-1-NH_2	41.2	0.09	S20

S3-1. Isosteric Heat of Adsorption

The adsorbate molecules (CO_2, CH_4, C_2H_2, C_2H_4 and C_2H_6) and the adsorbent lattice atoms is reflected in the isosteric heat of adsorption (Q_{st}) using Virial 2 model, which define as:

$$lnP = lnN + 1/T\sum_{i=0}^{m} a_i N^i + \sum_{i=0}^{n} b_i N^i \quad (1)$$

$$Q_{st} = -R\sum_{i=0}^{m} a_i N^i \quad (2)$$

Here, Q_{st} is the coverage-dependent enthalpy of adsorption, P is the pressure (mmHg), N is the adsorbed amount (mg/g), T is the temperature (K), a_i and b_i are virial coefficients, and m and N represent the number of coefficients used to describe the isotherms. Q_{st} is the coverage–dependent

enthalpy of adsorption and R is the universal gas constant. A virial-type equation (**1**) was used to fit adsorption data at 273 K and 298 K, and then the values of a_0 through a_m were used to calculate the isosteric heat of adsorption using equation (**2**).

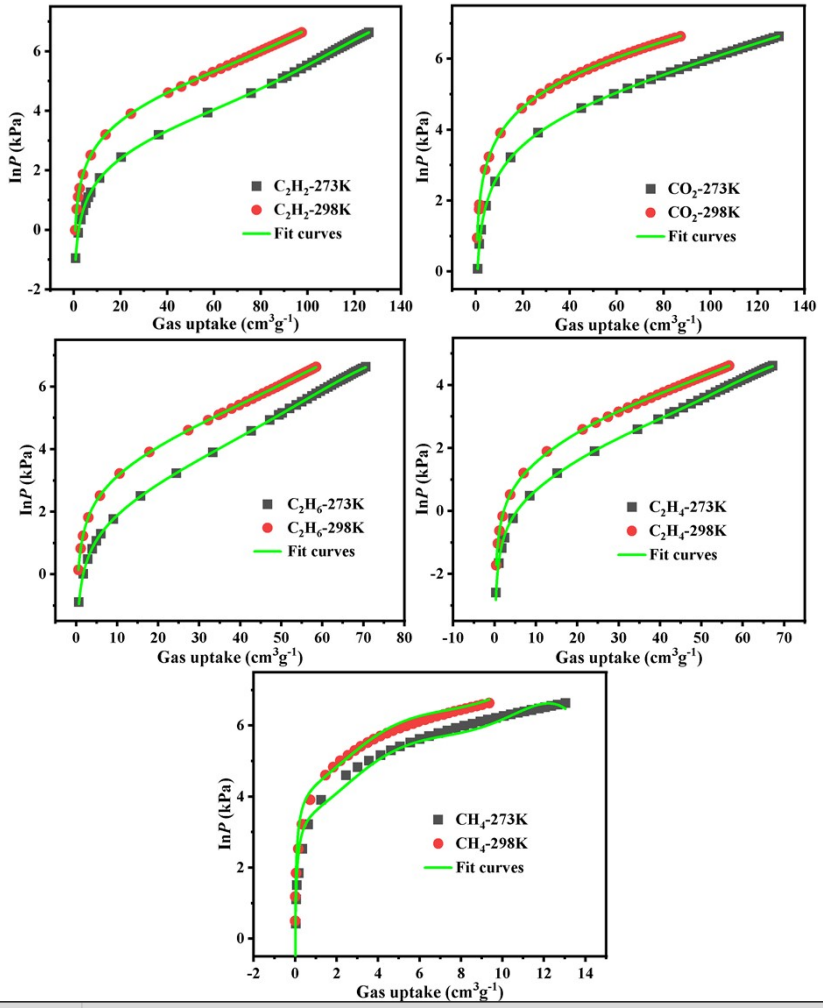

Model	Q_{st} (User)				
Equation	y=ln(x)+1/K*(a0+a1*x+a2*x^2+a3*x^3+a4*x^4+a5*x^5)+(b0)				
Plot	C_2H_2-298K	CO_2-298K	C_2H_6-298K	C_2H_4-298K	CH_4-298K
a0	-3952.70986	-3489.14808	-3633.91412	-3608.9671	-2125.6155
a1	-9.8061	6.42307	2.99682	10.98306	-364.03645
a2	0.15103	-0.0061	0.66592	0.81971	158.88258
a3	-0.0016	$1.49673*10^{-4}$	-0.0148	-0.01677	-28.32673
a4	$1.64845*10^{-5}$	$-2.59128*10^{-7}$	$2.21869*10^{-4}$	$2.51057*10^{-4}$	2.23417
b0	13.74304	$-1.06893*10^{-9}$	$-1.25616*10^{-6}$	$-1.40382*10^{-6}$	12.23594
b1	0.038	13.13678	12.76962	12.67893	-
Reduced Chi-Sqr	$1.26434*10^{-4}$	$1.25635*10^{-4}$	$1.1543*10^{-4}$	$1.40661*10^{-4}$	0.18227
R-Square (COD)	0.99997	0.99996	0.99997	0.99996	0.98538
Adj. R-Square	0.99995	0.99995	0.99997	0.99995	0.93463

Fig. S11 Virial fitting of C_2H_2, CO_2, C_2H_4, C_2H_6, and CH_4 adsorption isotherms (points) for Q_{st} calculation on **1a**.

S3-2. Ideal Adsorbed Solution Theory (IAST)

The experimental measured loadings for pure CO_2, CH_4, C_2H_2, C_2H_4 and C_2H_6 (measured at 273 and 298 K) in samples were fitted with a dual Langmuir-Freundlich (L-F) model (equation **3**):

$$q = \frac{a_1 * b_1 * p^{c_1}}{1 + b_1 * p^{c_1}} + \frac{a_2 * b_2 * p^{c_2}}{1 + b_2 * p^{c_2}} \quad (3)$$

Where q and p are adsorbed amounts per mass of adsorbent (mmol/g) and pressures of component i (kPa), respectively.

IAST calculations of adsorption selectivity for binary mixtures defined by equation **4**:

$$S_{i/j} = \frac{x_i * y_j}{x_j * y_i} \quad (4)$$

Where x_i and x_j are the molar loadings in the adsorbed phase in equilibrium with the bulk gas phase with partial pressures $y_{i,}$ and y_j. We calculate the values of x_i and x_j using IAST of Myers and Prausnitz.

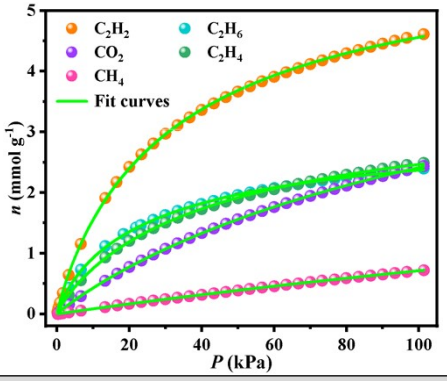

Model	LF (User)				
Equation	A1*b1*x^c1/(1+b1*x^c1)				
Plot	C_2H_6-298K	C_2H_4-298K	C_2H_2-298K	CO_2-298K	CH_4-298K
A1	3.1593 ± 0.03513	3.69706 ± 0.05025	6.23973 ± 0.06375	5.86577 ± 0.08138	4.43214 ± 0.44792
b1	0.05671 ± 0.0012	0.0324 ± $6.08126*10^{-4}$	0.04029 ± $7.93605*10^{-4}$	0.00886 ± $5.33928*10^{-5}$	0.00198 ± $1.40198*10^{-4}$
c1	0.86242 ± 0.01183	0.89557 ± 0.01108	0.91443 ± 0.01064	0.94839 ± 0.00488	0.99325 ± 0.01101
Reduced Chi-Sqr	$1.60115*10^{-4}$	$1.17711*10^{-4}$	$4.07429*10^{-4}$	$1.46286*10^{-5}$	$4.84442*10^{-6}$
R-Square (COD)	0.99975	0.99984	0.99985	0.99998	0.99991
Adj. R-Square	0.99974	0.99983	0.99984	0.99998	0.99991

Fig. S12 Single-site Langmuir-Freundlich fitting (red lines) of C_2H_2, CO_2, C_2H_4, C_2H_6, and CH_4 adsorption isotherms (black points) on **1a** at 298 K.

S3-3. Dynamic Gas Breakthrough Experiments

The mixed-gas breakthrough separation experiment was measured at 296 K using a lab scale fix-bed reactor. The as-synthesized sample 0.985 g of **1**a (985 mg) was degasified in-situ in the column through vacuuming at 333 K for 6 h before the measurement. A helium flow (10 mL/min) was used after the activation process to purge the adsorbent. The flow of He was then turned off, while a gas mixture of 50% C_2H_2, 50% CO_2 at 1 mL/min was allowed to flow into the column. The outlet composition was continuously monitored by gas chromatograph until complete breakthrough was achieved. On the basis of the gas balance, the gas adsorption capacities can be determined as follows:

$$q_i = \frac{C_i V}{22.4 \times m} \times \int_0^t (1 - \frac{F}{F_0}) dt \quad (5)$$

Where *qi* is the equilibrium adsorption capacity of gas *i* (mmol/g), *Ci* is the feed gas concentration, *V* is the volumetric feed flow rate (cm^3/min), *t* is the adsorption time (min), F_0 and *F* are the inlet and outlet gas molar flow rates, respectively, and m is the mass of the adsorbent (g).

The separation factor (α) of the breakthrough experiment is determined as:

$$\alpha = \frac{q_1 y_2}{q_2 y_1} \quad (6)$$

In which y_i is the molar fraction of gas *i* in the gas mixture.

S3-4. GCMC Computational Details

Grand canonical Monte Carlo (GCMC) simulations were modeled for the gas adsorption by using RASPA.[1] The 2×2×2 unit cell of framework with rigid structure was employed, and the Q_{eq} method was used to fit the partial charges of all atoms in the framework. The interaction energies between the gas molecules and framework were computed through the Coulomb and Lennard-Jones (LJ) potentials. All parameters of the host-guest interaction behavior were modeled with the universal force field (UFF). A cutoff distance of 12 Å was used for LJ interactions, and Ewald summation was employed to compute the Coulombic interactions. The 5×10^6 maximum loading steps and 5×10^6 production steps were employed for each run.

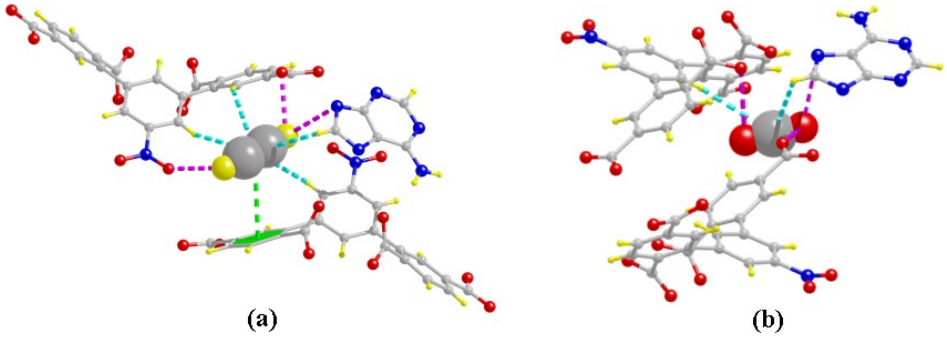

Fig. S13 Optimum adsorption sites for C_2H_2 (a) and CO_2 (b) in **1a**.

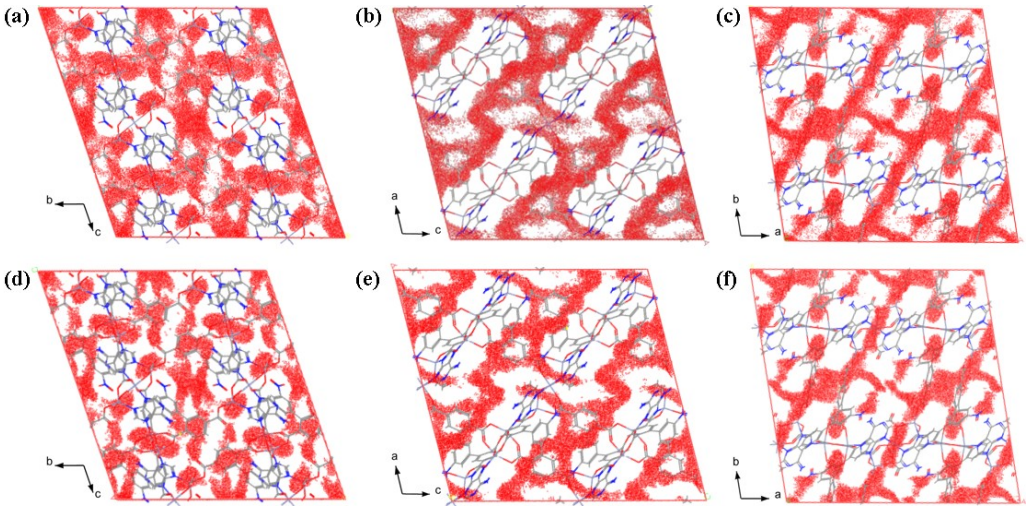

Fig. S14 Simulated probability density distribution profile of C_2H_2 (a-c) and CO_2 (d-f) in **1a** by GCMC simulation at 100 kPa and 298 K. (Note: C_2H_2 was more concentrated in the voids of the adsorbent than CO_2, which was compatible with experimental results.)

S4. References of Supplementary Information

1. D. Dubbeldam, S. Calero, D. E. Ellis and R. Q. Snurr, *Mol. Simul.*, 2016, **42**, 81-101.
2. K. Shao, H. M. Wen, C. C. Liang, X. Xiao, X. W. Gu, B. Chen, G. Qian and B. Li, *Angew. Chem., Int. Ed.*, 2022, **61**, e202211523.
3. Y. Ye, S. Xian, H. Cui, K. Tan, L. Gong, B. Liang, T. Pham, H. Pandey, R. Krishna, P. C. Lan, K. A. Forrest, B. Space, T. Thonhauser, J. Li and S. Ma, *J. Am. Chem. Soc.*, 2021, **144**, 1681-1689.
4. H. Yang, Y. Chen, C. Dang, A. N. Hong, P. Feng and X. Bu, *J. Am. Chem. Soc.*, 2022, **144**, 20221-20226.
5. W. Fan, S. Yuan, W. Wang, L. Feng, X. Liu, X. Zhang, X. Wang, Z. Kang, F. Dai, D. Yuan, D. Sun and H.-C. Zhou, *J. Am. Chem. Soc.*, 2020, **142**, 8728-8737.
6. P. Li, Y. Wang, Y. Y. Xue, H. P. Li, Q. G. Zhai, S. N. Li, Y. C. Jiang, M. C. Hu and X. Bu, *Angew. Chem., Int. Ed.*, 2019, **131**, 13724-13729.
7. F. Luo, C. Yan, L. Dang, R. Krishna, W. Zhou, H. Wu, X. Dong, Y. Han, T.-L. Hu, M. O'Keeffe, L. Wang, M. Luo, R.-B. Lin and B. Chen, *J. Am. Chem. Soc.*, 2016, **138**, 5678-5684.
8. N. Kumar, S. Mukherjee, N. C. Harvey-Reid, A. A. Bezrukov, K. Tan, V. Martins, M. Vandichel, T. Pham, L. M. van Wyk, K. Oyekan, A. Kumar, K. A. Forrest, K. M. Patil, L. J.

Barbour, B. Space, Y. Huang, P. E. Kruger and M. J. Zaworotko, *Chem*, 2021, **7**, 3085-3098.
9. J. Pei, H. M. Wen, X. W. Gu, Q. L. Qian, Y. Yang, Y. Cui, B. Li, B. Chen and G. Qian, *Angew. Chem., Int. Ed.*, 2021, **60**, 25068-25074.
10. J. Pei, K. Shao, J. X. Wang, H. M. Wen, Y. Yang, Y. Cui, R. Krishna, B. Li and G. Qian, *Adv. Mater.*, 2020, **32**, 1908275.
11. L. Wang, W. Sun, Y. Zhang, N. Xu, R. Krishna, J. Hu, Y. Jiang, Y. He and H. Xing, *Angew. Chem., Int. Ed.*, 2021, **60**, 22865-22870.
12. H. P. Li, Z. D. Dou, Y. Xiao, G. J. Fan, D. C. Pan, M. C. Hu and Q. G. Zhai, *Nanoscale*, 2022, **14**, 18200-18208.
13. J. Lee, C. Y. Chuah, J. Kim, Y. Kim, N. Ko, Y. Seo, K. Kim, T. H. Bae and E. Lee, *Angew. Chem., Int. Ed.*, 2018, **130**, 7995-7999.
14. J. Cui, Z. Qiu, L. Yang, Z. Zhang, X. Cui and H. Xing, *Angew. Chem., Int. Ed.*, 2022, **134**, e202208756.
15. R. B. Lin, L. Li, H. Wu, H. Arman, B. Li, R. G. Lin, W. Zhou and B. Chen, *J. Am. Chem. Soc.*, 2017, **139**, 8022-8028.
16. H. Zeng, M. Xie, Y. L. Huang, Y. Zhao, X. J. Xie, J. P. Bai, M. Y. Wan, R. Krishna, W. Lu and D. Li, *Angew. Chem., Int. Ed.*, 2019, **58**, 8515-8519.
17. W. Fan, S. B. Peh, Z. Zhang, H. Yuan, Z. Yang, Y. Wang, K. Chai, D. Sun and D. Zhao, *Angew. Chem., Int. Ed.*, 2021, **60**, 17338-17343.
18. Z. Zhang, S. B. Peh, Y. Wang, C. Kang, W. Fan and D. Zhao, *Angew. Chem., Int. Ed.*, 2020, **132**, 19089-19094.
19. L. Zhang, K. Jiang, L. Yang, L. Li, E. Hu, L. Yang, K. Shao, H. Xing, Y. Cui, Y. Yang, B. Li, B. Chen and G. Qian, *Angew. Chem., Int. Ed.*, 2021, **133**, 16131-16138.
20. L. Yang, L. Yan, Y. Wang, Z. Liu, J. He, Q. Fu, D. Liu, X. Gu, P. Dai, L. Li and X. Zhao, *Angew. Chem., Int. Ed.*, 2021, **133**, 4620-4624.